



**HAL**  
open science

# Vapor-to-glass preparation of biaxially aligned organic semiconductors

Jianzhu Ju, Debaditya Chatterjee, Paul Voyles, Harald Bock, Mark Ediger

► **To cite this version:**

Jianzhu Ju, Debaditya Chatterjee, Paul Voyles, Harald Bock, Mark Ediger. Vapor-to-glass preparation of biaxially aligned organic semiconductors. *The Journal of Chemical Physics*, 2023, 159 (21), pp.211101. 10.1063/5.0174819 . hal-04537659

**HAL Id: hal-04537659**


**<https://hal.science/hal-04537659>**

Submitted on 8 Apr 2024

**HAL** is a multi-disciplinary open access archive for the deposit and dissemination of scientific research documents, whether they are published or not. The documents may come from teaching and research institutions in France or abroad, or from public or private research centers.

L'archive ouverte pluridisciplinaire **HAL**, est destinée au dépôt et à la diffusion de documents scientifiques de niveau recherche, publiés ou non, émanant des établissements d'enseignement et de recherche français ou étrangers, des laboratoires publics ou privés.

# Vapor-to-glass preparation of biaxially aligned organic semiconductors

Jianzhu Ju,<sup>1,a)</sup>  Debaditya Chatterjee,<sup>2</sup>  Paul M. Voyles,<sup>2</sup>  Harald Bock,<sup>3</sup>  and Mark D. Ediger<sup>1,a)</sup> 

<sup>1</sup> Department of Chemistry, University of Wisconsin-Madison, Madison, Wisconsin 53706, USA

<sup>2</sup> Department of Materials Science and Engineering, University of Wisconsin-Madison, Madison, Wisconsin 53706, USA

<sup>3</sup> Centre de Recherche Paul Pascal, CNRS & Université de Bordeaux, 33600 Pessac, France

## ABSTRACT

Physical vapor deposition (PVD) provides a route to prepare highly stable and anisotropic organic glasses that are utilized in multi-layer structures such as organic light-emitting devices. While previous work has demonstrated that anisotropic glasses with uniaxial symmetry can be prepared by PVD, here, we prepare *biaxially* aligned glasses in which molecular orientation has a preferred in-plane direction. With the collective effect of the surface equilibration mechanism and template growth on an aligned substrate, macroscopic biaxial alignment is achieved in depositions as much as 180 K below the clearing point  $T_{LC-iso}$  (and 50 K below the glass transition temperature  $T_g$ ) with single-component disk-like (phenanthroperylene ester) and rod-like (itraconazole) mesogens. The preparation of biaxially aligned organic semiconductors adds a new dimension of structural control for vapor-deposited glasses and may enable polarized emission and in-plane control of charge mobility.

## INTRODUCTION

Physical vapor deposition (PVD)<sup>1,2</sup> provides a unique approach for preparing glassy materials with exceptional kinetic stability<sup>1,3-5</sup> and anisotropic order.<sup>6,7</sup> Molecular orientation can be tuned over a wide range by controlling the substrate temperature and deposition rate.<sup>3,8,9</sup> PVD has an additional advantage for the production of multilayer structures, where the solid-state preparation of individual layers below the glass transition temperature ( $T_g$ ) avoids the dissolving or melting of previously deposited layers.<sup>10-12</sup> PVD is widely applied in the production of organic light-emitting diodes (OLEDs). Uniaxially anisotropic glassy structures have proven advantageous in OLEDs, by increasing charge mobility<sup>13,14</sup> and outcoupling efficiency.<sup>15-17</sup> In addition, the high kinetic stability of PVD glasses has been shown to increase device lifetime.<sup>18</sup>

Previous works<sup>3,6,8,19</sup> have described how uniaxial anisotropic molecular packing and high kinetics stability are generated in PVD glasses through a surface equilibration mechanism. Molecules at the surface of organic glasses possess enhanced mobility<sup>1,9,20,21</sup> and this mobility allows partial equilibration during deposition.

Since this efficient equilibration occurs below the conventional  $T_g$ , it can lead to glass that has low enthalpy, high density, and high kinetic stability. Equilibration during deposition also produces packing arrangements that are generally anisotropic because the equilibration takes place in an anisotropic environment (the free surface). After being buried by subsequent deposition, molecules lose their high mobility and are locked in packing arrangements preferred at the surface.<sup>6,22</sup> Deposition rate and substrate temperature control the final anisotropic structure of the glass because these parameters control the extent to which equilibration occurs at the free surface during deposition.<sup>8,23,24</sup> As the result of this free surface effect, the anisotropy of PVD glasses exhibits *uniaxial* symmetry with respect to the surface normal. For example, rod-like molecules in PVD prefer vertical orientation at high substrate temperature  $T_{sub}$  and horizontal orientation at low  $T_{sub}$ : In both cases, macroscopic samples are isotropic in-plane.<sup>8,9,25</sup>

The existence of uniaxially anisotropic glasses naturally leads to the question of whether an even greater degree of anisotropic order can be prepared via PVD: Can we prepare *biaxially* anisotropic glasses? Molecules in a biaxial PVD film would have a preferred

in-plane orientation, in addition to having a preferred orientation with respect to the surface normal. Beyond the fundamental challenge, we expect that PVD preparation of biaxial glassy anisotropy can lead to new material properties that will enable new devices. A potential route to obtain biaxial glassy structures is to combine the surface equilibration mechanism with an additional physical mechanism to control alignment along different in-plane directions. Template growth is a method often applied to prepare crystalline nanostructures with well-controlled morphology and structural properties.<sup>26–28</sup> It takes advantage of an epitaxial interaction between the substrate and the molecules, which is not present for typical PVD depositions.<sup>29</sup> To use template growth as an additional control mechanism for anisotropy in organic materials, in this work, we propose to use PVD to deposit glass-forming mesogens<sup>30</sup> onto an in-plane alignment substrate. The interactions of mesogens (i.e., liquid crystal molecules) with substrates have been widely studied in their fluid (i.e., non-glassy) liquid crystalline mesophase,<sup>31–34</sup> where typically a thick mesogen layer over a few micrometers can be macroscopically aligned between pre-orientated parallel substrates.<sup>35–38</sup> As we describe below, PVD deposition onto an alignment substrate is distinct from this because a thin film is formed directly in the solid state, which is a key advantage. It is well established that mobility during PVD of glassy materials at temperatures below  $T_g$ <sup>9,25</sup> is limited to the free surface (within a few nanometers).<sup>3,8</sup> We envision that this mobility allows the initially deposited molecules to be aligned by the substrate. Each layer of deposited mesogens should then behave as a template layer for the alignment of the following mesogens during PVD, with the entire film growth occurring below  $T_g$ .

Here, we show that PVD can combine the surface equilibration mechanism with template growth in order to produce thin films of biaxially aligned organic semiconductors. We quantify the degree of biaxial order with x-ray scattering and polarized microscopy. We show that the successful control of biaxial order for the entire thickness of a deposited glass requires that the deposited mesogens have the capability to: (1) interact with the in-plane alignment substrate during initial deposition of mesogens; (2) maintain the in-plane alignment in subsequent deposition, i.e., template growth in the glassy state; and (3) retain the control of molecular orientation with respect to the surface normal, as controlled by the surface equilibration mechanism. The preparation of biaxially aligned organic semiconductors may provide new functionality for organic electronics, including polarized emission and in-plane control of charge mobility.

## MATERIAL AND METHODS

As the alignment substrate, polycarbonate ( $M_w = 64\,000$  g/mol) was dissolved by stirring overnight in dichloromethane at a concentration of 2 wt. %. Spin coating was performed at the rate of 6000 rpm for 1 min. Then, the wafers were kept in the fume hood for more than 5 h to evaporate the solvent and form a better attachment with the PC layer. The thickness of the PC layer is around 130 nm, measured by an M-2000U spectroscopic ellipsometer from J.A. Woollam Co., Inc. The bottom surface of a 500 g weight was covered with velvet cloth (Buehler MasterTex polishing cloth) to generate the oriented polymer surface. To apply reproducible rubbing, the weight was slid horizontally along the wafer unidirectionally, for around 1 s

per pass. The procedure provides a constant pressure of 1000 Pa and a rubbing speed of  $\sim 2.5$  cm/s. Rubbing results in grooves at an interval of 500 nm to 1  $\mu\text{m}$ , with a depth of a few nanometers [Fig. S2(c)], observable by atomic force microscopy (in Fig. S2 in supplementary material).

The physical vapor deposition (PVD) process has been described in detail elsewhere.<sup>7</sup> PVD was performed in a vacuum chamber with pressure around  $10^{-7}$  Torr. The source was heated at the bottom of the chamber to produce vapor and the deposition rate is monitored with a quartz crystal microbalance (QCM), with a precision of 0.01 nm/s. The synthesis of phenanthroperylene ester has been described in detail in Ref. 39. Itraconazole was purchased from Sigma-Aldrich and used as received. Substrates were adhered with Apiezon H grease to temperature-controlled copper blocks to achieve different  $T_{sub}$ .

The 4D-STEM measurements have been described in detail elsewhere.<sup>40</sup> Phenanthroperylene ester was deposited on a grid with an ultrathin carbon layer (5–6 nm) on top (CF400-CU, Electron Microscopy Sciences). Orientation mapping was performed with a 200 kV Thermo Fisher FEI Titan microscope in  $\mu\text{P}$  EFSTEM mode. The diffraction patterns were collected using a Direct Electron Celeritas detector with a  $256 \times 256$  readout area and a resolution of  $q = 0.314$  nm<sup>-1</sup>. Spatially resolved diffraction patterns were azimuthally integrated in the range of  $q = 17\text{--}20.7$  nm<sup>-1</sup> and then fitted to obtain the orientation maps. The domain size was estimated by orientation correlation  $C$ , as shown in the supplementary material.

Grazing incidence wide angle x-ray scattering (GIWAXS) for static measurements were performed in Stanford Synchrotron Radiation Light (SSRL) source on Beamline 11–3, with a wavelength of 0.0976 nm. The distance between the sample and detector was 317 mm, calibrated with LaB<sub>6</sub>. The measurements were performed in a helium atmosphere at around room temperature, with an exposure time of 60 s per image. The beam size is  $0.15 \times 0.15$  mm<sup>2</sup>, and the sample is reciprocated in 4 mm range perpendicularly to the direction of incidence. With a grazing-incidence angle of  $0.2^\circ$ , the detected diffraction is averaged in a narrow region with a width of 4 mm across the whole sample (over 25 mm), i.e., a macroscopic region. The incidence angle is  $0.2^\circ$  for all samples and all raw diffraction patterns were “ $\chi$  corrected,” resulting in the missing wedge.<sup>41</sup> The diffraction from PC was removed as background for all patterns shown in the paper.

Polarized reflected light microscopy was performed with Olympus BX51 in reflection mode. With the polarizer and analyzer perpendicular to each other, the maximum and minimum reflected intensities (transmitted twice through the film) can be obtained when the polarizer is  $45^\circ$  and  $0^\circ$  to the rubbing direction, respectively.

## MOLECULAR ORIENTATION CAN BE TEMPLATED DURING PVD

A critical feature of our proposed alignment mechanism is the capability for templating the alignment during deposition into the glassy state, so we first demonstrate that this is physically possible. A discotic mesogen, phenanthroperylene ester<sup>39</sup> (phen-ester for simplicity), is chosen as the model mesogen. For deposition at high substrate temperature  $T_{sub}$  just below  $T_g = 392$  K, phen-ester forms

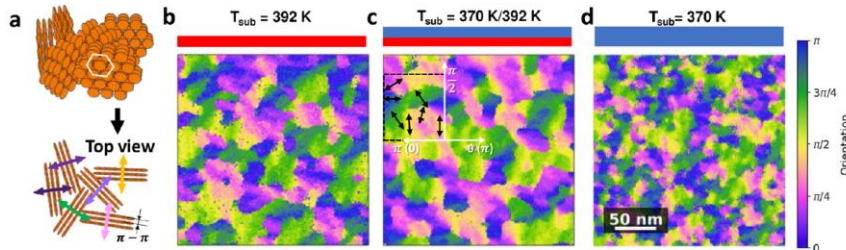


**FIG. 1.** (a) Schematic of phen-ester hexagonal columnar phase, as produced by PVD on an isotropic substrate at high  $T_{sub}$ . The top view image corresponds to the observation by 4D-STEM where the orientation of  $\pi$ - $\pi$  stacking can be mapped with a spatial resolution of 2 nm. Orientation maps are plotted in a field of 252 nm for PVD glasses prepared at  $T_{sub}$  of (b) 392 K, (c) 370 K on 392 K (bilayer film), and (d) 370 K. A small region in panel (c) indicates the orientation of individual domains with black arrows.

a hexagonal columnar mesophase, with edge-on molecular orientation [Fig. 1(a)].<sup>7,8</sup> Previous work used four-dimensional scanning transmission electron microscopy (4D-STEM) to show that the in-plane molecular orientation forms nanoscale domains 10–20 nm across.<sup>40</sup> Based on that capability, we demonstrate here that in-plane mesogen alignment can be transferred through many layers of subsequently deposited material.

Figure 1(b) shows that phen-ester is deposited onto ultrathin TEM grids with  $T_{sub} = 392$  K and a deposition rate of 0.03 nm/s to produce a 20 nm thick film. Orientation mapping of  $\pi$ - $\pi$  stacking can be obtained by spatially resolving the diffraction patterns. Domains with uniform orientation can be detected. The characteristic domain size is  $13 \pm 1$  nm, as calculated by the method described in Ref. 40 and shown in the supplementary material. We emphasize that the observed domains are three-dimensional and extend throughout the film's thickness.<sup>40</sup> When we use the 392 K deposited phen-ester film [a separate one than that in Fig. 1(b)] as a substrate to prepare a secondary 20 nm thick layer at  $T_{sub} = 370$  K, the bilayer film shows a similar domain size of  $15 \pm 1$  nm [Fig. 1(c)]. In contrast, deposition of a 40 nm thick film at 370 K produces smaller domains of  $8 \pm 1$  nm [see Fig. 1(d) and also results in Ref. 40].

The results in Fig. 1(c) clearly show that the bottom 392 K layer with large domains templates the local orientation of the top layer at  $T_{sub} = 370$  K. The successful templating observed here in the robust solid mesophase ( $T_g \sim 20$  K) is a surface effect enabled by high surface mobility, which distinguishes it from templating in a fluid mesophase. For bulk liquid crystals, the high mobility required for global self-assembly can only be achieved at temperatures close to clearing temperature  $T_{LC-iso}$ <sup>42,43</sup> (520 K for phen-ester<sup>44</sup>).

## MACROSCOPIC ALIGNMENT OF MESOGEN ORIENTATION

Having verified that orientation templating occurs locally during PVD, we attempted to prepare thin films with a macroscopic in-plane orientation by depositing them onto an alignment substrate, as described in the Materials and Methods section. The alignment sub-

strate was prepared by spin-coating polycarbonate (PC) with 130 nm thickness onto a 25 mm diameter silicon wafer, followed by mechanical rubbing. Phen-ester of 250 nm thickness was deposited onto the PC layer at different  $T_{sub}$ , at a deposition rate of 0.06 nm/s. Mechanical rubbing results in a grooved surface with thickness fluctuation in a scale of a few nanometers (as seen in the AFM measurements in Fig. S2 in supplementary material), which is much smaller than the deposited layer, so that it can be safely neglected. The in-plane anisotropy of the deposited phen-ester was measured with grazing-incidence wide-angle x-ray scattering (GIWAXS) by rotating the sample.

GIWAXS patterns verifying macroscopic in-plane mesogen orientation are shown in Fig. 2(a). The diffraction from PC was removed as background for all patterns shown in the paper. The in-plane angle between the x-ray beam and the rubbing direction is denoted as  $\psi_{view}$ , where  $\psi_{view} = 0^\circ$  when the beam is parallel to the rubbing direction [Fig. 2(b)]. At  $T_{sub} = 392$  K, for both  $\psi_{view} = 0^\circ$  and  $90^\circ$ , the hexagonal columnar phase can be detected with spot-like patterns at  $\chi$  of  $0^\circ$  and  $60^\circ$ , respectively ( $\chi = 0^\circ$  is defined to be along  $q_z$ <sup>8</sup>), at  $q$  around  $4 \text{ nm}^{-1}$ ; we designate the peak at  $\chi = 60^\circ$  as Peak H.  $\pi$ - $\pi$  stacking gives rise to a peak at  $q = 18 \text{ nm}^{-1}$  along  $q_{xy}$  at small  $q_z$ , and we designate this as Peak  $\pi$ . Considering both patterns, we confirm that the hexagonal columnar phase with edge-on molecule orientation is formed similar to that formed on an isotropic substrate at high  $T_{sub}$ ,<sup>8</sup> as shown in Fig. S3. Remarkably, Peak H is much brighter at  $\psi_{view} = 0^\circ$  and Peak  $\pi$  is much brighter at  $\psi_{view} = 90^\circ$ . From this result, the anisotropic packing of the hexagonal columnar phase can be understood, with most of the columns propagating along the rubbing direction. [For perfect alignment [schematically shown in Fig. 2(b)], Peak H would only be observed at  $\psi_{view} = 0^\circ$  and Peak  $\pi$  only at  $\psi_{view} = 90^\circ$ .] The anisotropy is also observed for deposition at 370 K, as shown in Fig. 2(a). At  $T_{sub}$  below 370 K, the hexagonal columnar packing is barely identifiable, and the diffraction patterns are identical at all  $\psi_{view}$  (Fig. S4). In summary of the GIWAXS patterns, a macroscopically biaxial anisotropy can be obtained by PVD on an alignment substrate well below  $T_{LC-iso}$  and even in glass state below  $T_g$ . Importantly, we observe a highly anisotropic structure in a film with a thickness of 250 nm. This extends the results of the 4D-STEM measurements [Fig. 1(b)], which

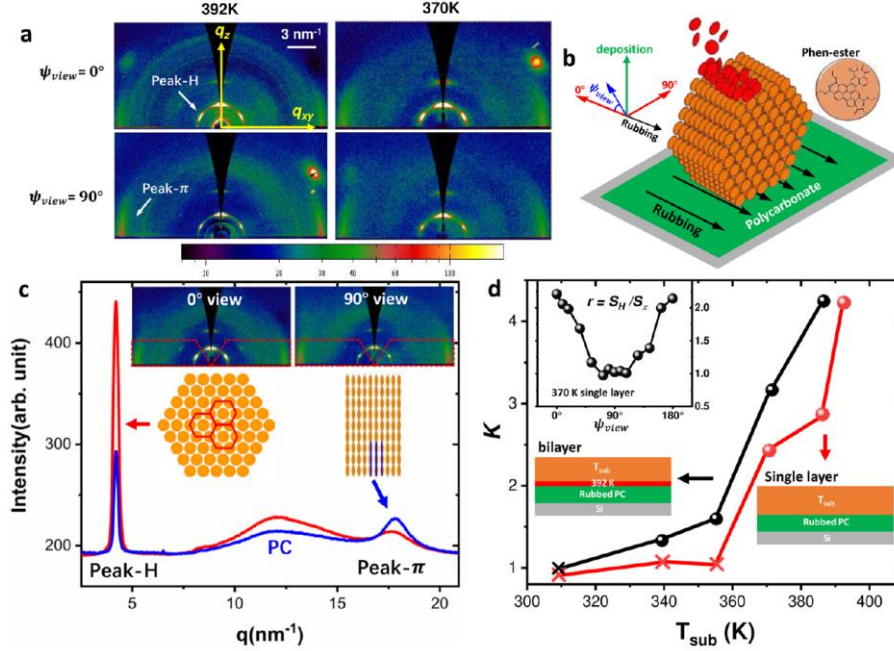


**FIG. 2.** (a) GIWAXS patterns at different  $T_{sub}$  with  $\psi_{view} = 0^\circ$  and  $90^\circ$ . (b) Schematic of the biaxial alignment of phen-ester. (c) 1D intensity as the function of  $q$  for 386 K bilayer (integrated in the region marked in the inset). The curves are normalized to the intensity at  $q = 30 \text{ nm}^{-1}$ . Inset: GIWAXS patterns and schematic drawing at  $0^\circ$  and  $90^\circ$  views. (d) Orientation parameter  $K$  as the function of  $T_{sub}$  for single layers (red) and bilayers (black). Inset curve: Peak area ratio  $S_H/S_\pi$  as a function of  $\psi_{view}$  for 370 K single layer.

demonstrated effective templating through the thickness of 40 nm films.

Inspired by the 4D-STEM observation in Fig. 1, we tested whether the macroscopic alignment efficiency can be further improved by introducing a thin template layer deposited at higher  $T_{sub}$ . The deposition of the bilayer films follows two steps: First, a 30 nm layer of phen-ester is deposited onto the PC alignment substrate at  $T_{sub} = T_g = 392 \text{ K}$  as a templating layer, and then a 220 nm layer is deposited onto the templating layer at different  $T_{sub}$ . To quantitatively characterize the macroscopic alignment, the averaged intensity as a function of  $q$  is calculated. [The intensity is averaged in the region indicated in Fig. 2(c) with  $q_z < 3.7 \text{ nm}^{-1}$  and excluding the region containing the vertical peak at  $q$  around  $4 \text{ nm}^{-1}$  ( $-30^\circ < \chi < 30^\circ$ ), which is contributed from all  $\psi_{view}$ .] The 1D intensity curves for the bilayer at  $T_{sub} = 386 \text{ K}$  (on top of thin 392 K layer) at different  $\psi_{view}$  are shown in Fig. 2(c). Significant and *opposite* changes in the intensity of Peaks H and  $\pi$  can be observed. Peak areas  $S_H$  and  $S_\pi$  can be fitted from 1D intensities (details shown in Fig. S5). The wide peak at  $q \sim 13 \text{ nm}^{-1}$  is related to PC and can be well-separated from  $S_H$  and  $S_\pi$ . The ratio  $r(\psi_{view}) = S_H/S_\pi$  is a characteristic parameter for in-plane anisotropy, with the two peaks having opposite dependences on  $\psi_{view}$ . Higher  $r$  means a larger number of hexagonal columns propagating in the direction of the x-ray beam.  $r(\psi_{view})$  for

the single layer deposition at  $T_{sub} = 370 \text{ K}$  is plotted in the inset of Fig. 2(d), where more than a two-fold change can be observed. The macroscopic alignment is quantified by an anisotropy parameter  $K$ , which increases with in-plane anisotropy,

$$K = \frac{r(0^\circ)}{r(90^\circ)} = \frac{S_{H0}S_{\pi90}}{S_{\pi0}S_{H90}}.$$

Figure 2(d) compares the anisotropy parameter  $K(T_{sub})$  in bilayers and single layers. In both series,  $K$  increases with  $T_{sub}$  from 1 (isotropic in-plane) at low temperature to 4.5 for  $T_{sub} \sim T_g$ . This is expected since the mesogens have higher mobility for better surface equilibration and template interaction when deposited at high  $T_{sub}$ .<sup>8,9</sup> By comparing the single layers and bilayers, even though 88% of the phen-ester is deposited at the same  $T_{sub}$ , we find that  $K$  for the bilayer is significantly larger than that for the single layers. A more common orientation parameter  $S_{2D}$  can be calculated from multi- $\psi_{view}$  measurements<sup>45</sup> as shown in Fig. S6 in supplementary material. For the sample with the highest orientation, the bilayer at  $T_{sub} = 386 \text{ K}$ , we estimate  $S_{2D} = 0.37$ , showing substantial anisotropy.

The superiority of bilayers over single layers is notable, given that all the observed in-plane anisotropy is ultimately derived from

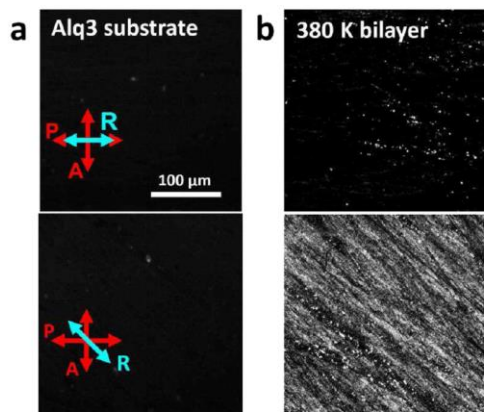


**FIG. 3.** Optical microscopy images utilizing crossed polarizers with the rubbing angle at 0° (top) and 45° (bottom) for (a) Alq<sub>3</sub> substrate and (b) 380 K phen-ester bilayer. The rubbed Alq<sub>3</sub> substrate is not birefringent, while the phen-ester overlayer is strongly birefringent (and thus aligned).

the same aligned PC substrate. We interpret this to mean that the substantial alignment shown in Fig. 2(d) is not limited by the choice of mesogen or by the PVD process and that even greater macroscopic anisotropy could be achieved with a substrate that more effectively aligns (in comparison to PC). The AFM measurements show that the 392 K template layer is smoother than the PC layer itself (Fig. S2 in supplementary material), emphasizing that the alignment efficiency observed in the bilayer samples is dominated by intramolecular interaction at the surface. Remarkably, the biaxial anisotropy can still be generated at 180 K below  $T_{LC-iso}$ , in contrast to conventional liquid crystal alignment.

Additional experiments show that conventional alignment in the fluid mesophase is impossible with this mesogen and substrate. We vapor-deposited phen-ester films on rubbed PC below  $T_g$  and then annealed at around 420 K while acquiring the GIWAXS data

(Fig. S9 in supplementary material). No alignment or rearrangement of the mesogens could be detected, as expected for annealing far below the clearing temperature (520 K). Higher annealing temperatures are not feasible, as annealing above the PC  $T_g$  (420 K<sup>46,47</sup>) destroys the alignment in the PC substrate. This illustrates a key advantage of our PVD approach. Even substrates with relatively low  $T_g$  values can be used for alignment. In addition, the present route produces alignment on films as thin as 20 nm without dewetting (Fig. 1). This cannot be achieved in the fluid mesophase because the high temperatures required for alignment also lead to dewetting.

### BIAXIAL ALIGNMENT BY ORGANIC SEMICONDUCTOR SUBSTRATE

To further test the feasibility of coupling biaxial alignment by PVD with multilayer device manufacturing, we show that alignment can also be achieved using an organic semiconductor as the substrate. A 300 nm layer of Alq<sub>3</sub> [tris(8-hydroxyquinoline) aluminum]<sup>48</sup> was vapor-deposited (at 340 K with a rate of 0.2 nm/s) onto the Si wafer and then rubbed with the process discussed above. On top of this, we vapor-deposited a 250 nm phen-ester bilayer (20 nm at 392 K, followed by 230 nm at 380 K). Optical anisotropy is quantified by the degree of polarization  $D$ , defined as

$$D = \frac{I_{\max} - I_{\min}}{I_{\max} + I_{\min}},$$

where  $I_{\max}$  and  $I_{\min}$  can be obtained when the crossed polarizers are 45° and 0° to the rubbing direction, respectively. As shown in Fig. 3(a), the rubbed Alq<sub>3</sub> substrate exhibits no birefringence in an optical microscope (presumably as a result of the molecule's nearly spherical symmetry<sup>48</sup>). On the other hand, in Fig. 3(b), strong birefringence can be observed in the 380 K bilayer, with  $D$  of 70%. The large birefringence observed when the phen-ester bilayer is present can be completely attributed to the in-plane orientation of phen-ester molecules, as expected for a strongly aligned sample. The GIWAXS measurements of the 380 K bilayer on Alq<sub>3</sub> (Fig. S7) confirm this interpretation, indicating that

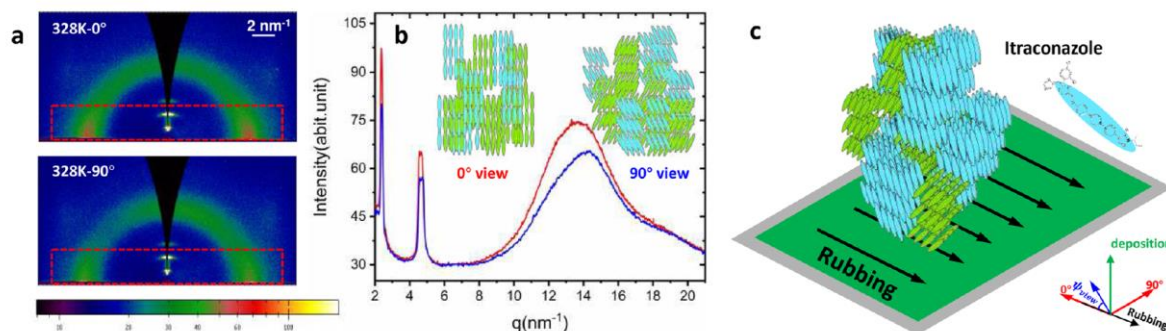


**FIG. 4.** (a) GIWAXS patterns of a rod-like mesogen, itraconazole, at  $\psi_{\text{view}} = 0^\circ$  and  $90^\circ$  with  $T_{\text{sub}} = T_g = 328$  K. (b) 1D intensity averaged in the region shown in (a). The inset shows the schematic of 0° and 90° views corresponding to GIWAXS patterns. (c) Schematic of the biaxial alignment of itraconazole.

$K = 2.7$ . All these observations indicate that biaxial alignment of semiconductor mesogens by PVD can be achieved with an underlying organic semiconductor substrate, and shows that PVD can effectively prepare well-aligned nanofilms with substantial optical anisotropy.

## BIAXIAL ALIGNMENT OF ROD-LIKE MESOGENS

The preparation route described above should be applicable for any mesogens with the ability to generate biaxial packing. Here, we show an additional example of solid-state biaxial alignment, with a rod-like mesogen, itraconazole. As reported in previous works,<sup>9,49</sup> at high  $T_{sub}$ , the deposition of itraconazole on an isotropic substrate generates a glass with uniaxial anisotropy, with mesogens tilted at an average angle around  $60^\circ$  from the substrate.<sup>49</sup> To achieve biaxial alignment, we deposited itraconazole at  $T_{sub} = T_g = 328$  K ( $T_{LC-iso} = 363$  K<sup>50</sup>) on rubbed PC. GIWAXS experiments with  $\psi_{view} = 0^\circ$  and  $90^\circ$  [Fig. 4(a)] show a layered structure (diffraction peaks at  $\chi = 0^\circ$  with first peak at  $q_z$  around  $2 \text{ nm}^{-1}$ ) with overall vertical mesogen orientation ( $\pi$ - $\pi$  stacking peaks at  $\chi = 90^\circ$  and  $q_{xy}$  around  $14 \text{ nm}^{-1}$ ) can be observed. The horizontal peak is stronger at  $\psi_{view} = 0^\circ$ , indicating in-plane anisotropy. To avoid scattering from PC (see supplementary material), an averaging region containing mainly the in-plane peaks [indicated in Fig. 4(a)] is selected for quantitative comparison, with results shown in Fig. 4(b). The in-plane anisotropy results from the molecules preferentially tilting along the rubbing direction,<sup>49</sup> as schematically shown in Fig. 4(c). We expect that a perfectly aligned structure, at  $\psi_{view} = 0^\circ$ , would show no indication of tilting, while at  $\psi_{view} = 90^\circ$ , a tilted orientation would be detected [inset in Fig. 4(b)].

## CONCLUDING REMARKS

In this work, we report substantial progress toward the manufacture of *biaxially* aligned glasses by PVD. A glassy solid with in-plane alignment is directly synthesized at low temperature without utilizing equilibrium liquid crystalline phases. In this process, mesogens also exhibit out-of-plane orientation, which is similar to when they are deposited on isotropic substrates. In this way, the out-of-plane and in-plane orientations are *independently* governed by the free surface and the alignment substrate, respectively. A key parameter,  $T_{sub}$ , tunes the extent of equilibration for both out-of-plane and in-plane orientation.

The successful preparation of biaxially aligned glass makes use of the stimuli-responsiveness of mesogenic vapors to an oriented substrate. During PVD, this can occur below  $T_g$  as a result of high molecular mobility at the free surface of the growing film, and transfer of in-plane alignment from layer to layer via templating. This solid-state low temperature processing can achieve substantial alignment at up to 180 K below  $T_{LC-iso}$ , thus avoiding high temperature preparation. We have also shown that a thin glassy layer of the mesogen can be used as a template to better align the following layers. Such templating layers could be separately programmable (via  $T_{sub}$ ) during a continuous deposition, providing further process control to increase or decrease in-plane alignment.

At the current state of development, the preparation of a biaxially aligned glass depends on a pre-processed alignment substrate that cannot be adjusted *in situ*. More to this, mechanical

rubbing unavoidably increases surface roughness, which is unfavored in electronic devices with ultrathin layers. As a next step, strategies that allow programmed alignment inside a deposition chamber without mechanical rubbing will be explored. Strategies borrowed from bulk liquid crystals may be successful,<sup>51</sup> such as coupling electric and magnetic fields into the deposition system, or preparing an alignment layer with an anisotropic surface morphology that can be prepared by glancing angle vapor deposition.<sup>52-56</sup>

What are the prospects for using PVD to produce biaxial glasses of non-mesogens? In qualitative terms, glasses are not very good at propagating structure away from an interface because there are so many available packing arrangements. The packing arrangements of mesogens are sufficiently limited that the structure can be successfully propagated from the substrate, as shown in this work. It is an open question whether PVD of non-mesogens can be used to prepare biaxial glasses.

## SUPPLEMENTAL MATERIAL

Additional information is provided: (1) Data processing of 4D-STEM data; (2) AFM images showing surface morphology of the rubbed substrate; (3) GIWAXS analysis detail and additional GIWAXS results.

## ACKNOWLEDGMENTS

This work was supported by Wisconsin MRSEC (No. NSF DMR-1720415). The authors thank Xiaodan Gu and Guorong Ma for their advice and assistance with *in situ* GIWAXS measurements, and Dean DeLongchamp for the useful discussions. The use of the Stanford Synchrotron Radiation Lightsource at SLAC National Accelerator Laboratory was supported by the U.S. Department of Energy, Office of Science, Office of Basic Energy Sciences, under Contract No. DE-AC02-76SF00515.

## AUTHOR DECLARATIONS

### Conflict of Interest

The authors have no conflicts to disclose.

## Author Contributions

**Jianzhu Ju:** Conceptualization (equal); Formal analysis (equal); Investigation (equal); Methodology (equal); Visualization (equal); Writing – original draft (equal); Writing – review & editing (equal). **Debaditya Chatterjee:** Formal analysis (equal); Investigation (equal); Methodology (equal); Writing – review & editing (equal). **Paul M. Voyles:** Conceptualization (equal); Formal analysis (equal); Methodology (equal); Writing – review & editing (equal). **Harald Bock:** Conceptualization (equal); Investigation (equal); Methodology (equal); Writing – review & editing (equal). **Mark D. Ediger:** Conceptualization (equal); Formal analysis (equal); Funding acquisition (equal); Investigation (equal); Methodology

(equal); Project administration (equal); Resources (equal); Supervision (equal); Validation (equal); Visualization (equal); Writing – original draft (equal); Writing – review & editing (equal).

## DATA AVAILABILITY

ASCII and tif. format images in all the presented figures have been uploaded in Zenodo (DOI: [10.5281/zenodo.7747240](https://doi.org/10.5281/zenodo.7747240)).

## REFERENCES

- 1 S. F. Swallen, K. L. Kearns, M. K. Mapes, Y. S. Kim, R. J. McMahon, M. D. Ediger, T. Wu, L. Yu, and S. Satija, *Science* **315**, 353 (2007).
- 2 M. D. Ediger, *J. Chem. Phys.* **147**, 210901 (2017).
- 3 S. S. Dalal, D. M. Walters, I. Lyubimov, J. J. de Pablo, and M. D. Ediger, *Proc. Natl. Acad. Sci. U. S. A.* **112**, 4227 (2015).
- 4 K. L. Kearns, S. F. Swallen, M. D. Ediger, T. Wu, and L. Yu, *J. Chem. Phys.* **127**, 154702 (2007).
- 5 C. Rodriguez-Tinoco, M. Gonzalez-Silveira, M. A. Ramos, and J. Rodriguez-Viejo, *Riv. Nuovo Cimento* **45**, 325 (2022).
- 6 C. Bishop, J. L. Thelen, E. Gann, M. F. Toney, L. Yu, D. M. DeLongchamp, and M. D. Ediger, *Proc. Natl. Acad. Sci. U. S. A.* **116**, 21421 (2019).
- 7 A. Gujral, J. Gómez, S. Ruan, M. F. Toney, H. Bock, L. Yu, and M. D. Ediger, *Chem. Mater.* **29**, 9110 (2017).
- 8 C. Bishop, Z. Chen, M. F. Toney, H. Bock, L. Yu, and M. D. Ediger, *J. Phys. Chem. B* **125**, 2761 (2021).
- 9 C. Bishop, A. Gujral, M. F. Toney, L. Yu, and M. D. Ediger, *J. Phys. Chem. Lett.* **10**, 3536 (2019).
- 10 A. Ghosh, L. Gerenser, C. Jarman, and J. Fornalik, *Appl. Phys. Lett.* **86**, 223503 (2005).
- 11 G. Chen, Y. Weng, F. Sun, X. Zhou, C. Wu, Q. Yan, T. Guo, and Y. Zhang, *RSC Adv.* **9**, 20884 (2019).
- 12 A. Inspektor and P. A. Salvador, *Surf. Coat. Technol.* **257**, 138 (2014).
- 13 D. Yokoyama, H. Sasabe, Y. Furukawa, C. Adachi, and J. Kido, *Adv. Funct. Mater.* **21**, 1375 (2011).
- 14 W. Pisula, M. Zorn, J. Y. Chang, K. Müllen, and R. Zentel, *Macromol. Rapid Commun.* **30**, 1179 (2009).
- 15 K. H. Kim and J. J. Kim, *Adv. Mater.* **30**, 1705600 (2018).
- 16 M. Flämmich, J. Frischeisen, D. S. Setz, D. Michaelis, B. C. Krummacker, T. D. Schmidt, W. Brütting, and N. Danz, *Org. Electron.* **12**, 1663 (2011).
- 17 A. Hofmann, M. Schmid, and W. Brütting, *Adv. Opt. Mater.* **9**, 2101004 (2021).
- 18 J. Ràfols-Ribé, A. Vila-Costa, C. Rodriguez-Tinoco, A. F. Lopeandia, J. Rodriguez-Viejo, and M. Gonzalez-Silveira, *Phys. Chem. Chem. Phys.* **20**, 29989 (2018).
- 19 P. Harrowell, *Proc. Natl. Acad. Sci. U. S. A.* **116**, 21341 (2019).
- 20 Y. Li, W. Zhang, C. Bishop, C. Huang, M. Ediger, and L. Yu, *Soft Matter* **16**, 5062 (2020).
- 21 Y. Zhang and Z. Fakhraai, *Phys. Rev. Lett.* **118**, 066101 (2017).
- 22 C. Bishop, K. Bagchi, M. F. Toney, and M. D. Ediger, *J. Chem. Phys.* **156**, 014504 (2022).
- 23 C. Bishop, Y. Li, M. F. Toney, L. Yu, and M. Ediger, *J. Phys. Chem. B* **124**, 2505 (2020).
- 24 S. L. He, E. Pakhomenko, and R. J. Holmes, *ACS Appl. Mater. Interfaces* **15**, 1652 (2023).
- 25 J. Gómez, J. Jiang, A. Gujral, C. Huang, L. Yu, and M. Ediger, *Soft Matter* **12**, 2942 (2016).
- 26 A. L. Briseno, J. Aizenberg, Y.-J. Han, R. A. Penkala, H. Moon, A. J. Lovinger, C. Kloc, and Z. Bao, *J. Am. Chem. Soc.* **127**, 12164 (2005).
- 27 B. R. Heywood and S. Mann, *Adv. Mater.* **6**, 9 (1994).
- 28 Z. Lin, A. Yin, J. Mao, Y. Xia, N. Kempf, Q. He, Y. Wang, C.-Y. Chen, Y. Zhang, V. Ozolins *et al.*, *Sci. Adv.* **2**, e1600993 (2016).
- 29 J. Yang, D. Yan, and T. S. Jones, *Chem. Rev.* **115**, 5570 (2015).
- 30 M. Brewis and G. J. Clarkson, *Chem. Commun.* **9**, 969 (1998).
- 31 T. Yanagimachi, X. Li, P. F. Nealey, and K. Kurihara, *Adv. Colloid Interface Sci.* **272**, 101997 (2019).
- 32 G. Schwalb and F. W. Deeg, *Phys. Rev. Lett.* **74**, 1383 (1995).
- 33 J. A. Martinez-Gonzalez, X. Li, M. Sadati, Y. Zhou, R. Zhang, P. F. Nealey, and J. J. de Pablo, *Nat. Commun.* **8**, 15854 (2017).
- 34 Y. F. Li, J. Jun-Yan Suen, E. Prince, E. M. Larin, A. Klinkova, H. Therien-Aubin, S. J. Zhu, B. Yang, A. S. Helmy, O. D. Lavrentovich, and E. Kumacheva, *Nat. Commun.* **7**, 12520 (2016).
- 35 L. T. Creagh and A. R. Kmetz, *Mol. Cryst. Liq. Cryst.* **24**, 59 (1973).
- 36 J. Stöhr, M. Samant, J. Lüning, A. Callegari, P. Chaudhari, J. Doyle, J. Lacey, S. Lien, S. Purushothaman, and J. Speidell, *Science* **292**, 2299 (2001).
- 37 S. Ishihara, H. Wakemoto, K. Nakazima, and Y. Matsuo, *Liq. Cryst.* **4**, 669 (1989).
- 38 M. Nishikawa, B. Taheri, and J. L. West, *Appl. Phys. Lett.* **72**, 2403 (1998).
- 39 J. Kelber, M. F. Achard, F. Durola, and H. Bock, *Angew. Chem., Int. Ed.* **51**, 5200 (2012).
- 40 D. Chatterjee, S. Huang, K. Gu, J. Ju, J. Yu, H. Bock, L. Yu, M. D. Ediger, and P. M. Voyles, *Nano Lett.* **23**, 2009 (2023).
- 41 J. L. Baker, L. H. Jimison, S. Mannsfeld, S. Volkman, S. Yin, V. Subramanian, A. Salleo, A. P. Alivisatos, and M. F. Toney, *Langmuir* **26**, 9146 (2010).
- 42 J. Echer, G. C. Faria, H. Bock, H. von Seggern, and I. H. Bechtold, *ACS Appl. Mater. Interfaces* **5**, 11935 (2013).
- 43 O. Thiebaut, H. Bock, and E. Grelet, *J. Am. Chem. Soc.* **132**, 6886 (2010).
- 44 Z. Chen, C. Bishop, E. Thoms, H. Bock, M. D. Ediger, R. Richert, and L. Yu, *Chem. Mater.* **33**, 4757 (2021).
- 45 N. E. Persson, S. Engmann, L. J. Richter, and D. M. DeLongchamp, *Chem. Mater.* **31**, 4133 (2019).
- 46 N. Shamim, Y. P. Koh, S. L. Simon, and G. B. McKenna, *J. Polym. Sci., Part B: Polym. Phys.* **52**, 1462 (2014).
- 47 R. J. Morgan and J. E. O'Neal, *J. Polym. Sci., Polym. Phys. Ed.* **14**, 1053 (1976).
- 48 K. Bagchi, N. E. Jackson, A. Gujral, C. Huang, M. F. Toney, L. Yu, J. J. De Pablo, and M. Ediger, *J. Phys. Chem. Lett.* **10**, 164 (2018).
- 49 A. Gujral, J. Gómez, J. Jiang, C. Huang, K. A. O'Hara, M. F. Toney, M. L. Chabinyk, L. Yu, and M. D. Ediger, *Chem. Mater.* **29**, 849 (2017).
- 50 R. Teerakapibal, C. Huang, A. Gujral, M. D. Ediger, and L. Yu, *Phys. Rev. Lett.* **120**, 055502 (2018).
- 51 H. K. Bisoyi and Q. Li, *Prog. Mater. Sci.* **104**, 1 (2019).
- 52 P. C. Hruddy, K. L. Westra, and M. J. Brett, *Adv. Mater.* **18**, 224 (2006).
- 53 J. R. Sanchez-Valencia, R. Longtin, M. D. Rossell, and P. Gröning, *ACS Appl. Mater. Interfaces* **8**, 8686 (2016).
- 54 J. L. Janning, *Appl. Phys. Lett.* **21**, 173 (1972).
- 55 S. V. Roth, G. Santoro, J. F. H. Risch, S. Yu, M. Schwartzkopf, T. Boese, R. Dohrmann, P. Zhang, B. Besner, P. Bremer, D. Rukser, M. A. Rubhausen, N. J. Terrill, P. A. Staniec, Y. Yao, E. Metwalli, and P. Muller-Buschbaum, *ACS Appl. Mater. Interfaces* **7**, 12470 (2015).
- 56 M. Oliva-Ramirez, C. Lopez-Santos, F. Yubero, and A. R. Gonzalez-Elipe, *Adv. Mater. Interfaces* **5**, 1800530 (2018).